PHYSICAL REVIEW D **87,** 034508 (2013)

Orthogonal technicolor with isotriplet dark matter on the lattice

Ari Hietanen,[*] Claudio Pica,[†] Francesco Sannino,[‡] and Ulrik Ishøj Søndergaard[§]
CP^3*-Origins and the Danish Institute for Advanced Study DIAS, University of Southern Denmark, Campusvej 55, DK-5230 Odense M, Denmark*
(Received 6 December 2012; published 13 February 2013)

We study the gauge dynamics of an SO(4)-gauge theory with two Dirac Wilson fermions transforming according to the vector representation of the gauge group. We determine the lattice phase diagram by locating the strong coupling bulk phase transition line and the zero quark mass line. We present results for the spectrum of the theory obtained at a fixed value of the lattice spacing. In particular we measure the pseudoscalar, vector and axial meson masses. The data are consistent with a chiral symmetry breaking scenario rather than a conformal one. When used to break the electroweak symmetry dynamically the model leads to a natural dark matter candidate.

DOI: 10.1103/PhysRevD.87.034508 PACS numbers: 11.15.Ha, 11.30.Rd

I. INTRODUCTION

Understanding the phase diagram of strongly interacting theories will unveil a large number of theories of fundamental interactions useful to describe electroweak symmetry breaking, dark matter and even inflation [1–4]. To gain a coherent understanding of strong dynamics besides the SU(N) gauge groups [5,6], one should also investigate the orthogonal, symplectic and exceptional groups. SO(N) and SP(2N) phase diagrams were investigated with analytic methods in Ref. [7], while the exceptional ones together with orthogonal gauge groups featuring spinorial matter representationswere studied in Ref. [8]. So far lattice simulations have been mostly employed to explore the phase diagram of SU(N) gauge theories while a systematic lattice analysis of the smallest symplectic group was launched in Ref. [9].

Here we move forward by analyzing on the lattice the dynamics of the SO(4) gauge group with two Dirac fermions in the vector representation of the group. This choice is based on the following theoretical and phenomenological considerations. The theory is expected to be below or near the lower boundary of the conformal window [7,10], and therefore break chiral symmetry. The theory can be used as a technicolor [11,12] template similar, from the global symmetry point of view, to minimal walking technicolor (MWT) [5,13,14].

Although the chiral symmetry breaking pattern is identical to the one of MWT there are substantial differences in the massive spectrum of the theory with important phenomenological consequences. This is because for MWT the technifermions, like the technigluons, transform according to the adjoint representation of the underlying gauge group. Consequently, one can immediately construct technicolor gauge singlets, which are made from one technifermion and one techniglue. This forces model builders to choose nonstandard model hypercharge assignments for the technifermions in order to make sure that the composite fermonic states have integer electric charges. Furthermore, the Witten anomaly [15] of MWT is resolved by adding new leptonlike fermions that are doubly charged because of the hypercharge choice with interesting phenomenology. The theory we investigate here has the following features: Being an SO(4) gauge theory it has an even number of technifermions gauged under the electroweak avoiding the Witten anomaly; the technigluons belong to the two-index antisymmetric representation [the adjoint of SO(4)] while the technifermions to the vector representation, therefore forbidding the construction of a technifermion-technigluon bound state. These features renders *orthogonal technicolor* a simpler model than MWT.

Furthermore the orthogonal technicolor theory leads to a weak isotriplet with the neutral member being an ideal dark matter candidate [7,10], the isotriplet technicolor interactive massive particle (iTIMP). This state is a pseudo Goldstone and therefore can be light with respect to the electroweak scale making it a natural candidate to resolve some of the current experimental puzzles [10,16]. The first model featuring composite dark matter pions appeared in Refs. [17,18] and the first study of technipion dark matter on a lattice appeared in Ref. [9].

Due to the reality of the fermion representation the quantum global symmetry group is SU(4) expected to break spontaneously to SO(4), yielding nine Goldstone bosons. Once gauged under the electroweak theory three are eaten by the SM gauge bosons. Six additional Goldstone bosons form an electroweak complex triplet of technibaryon with the neutral isospin zero component to be identified with the iTIMP of Ref. [10].

SO(4) is a semisimple group, SO(4) $\cong$ SU(2) $\otimes$ SO(3), and it has a nontrivial center Z_2. The theory is asymptotically free and since the two-loop β-function for different number of flavors loses the infrared zero for $N_f = 2.3$

[*]hietanen@cp3-origins.net
[†]pica@cp3-origins.net
[‡]sannino@cp3.dias.sdu.dk
[§]sondergaard@cp3.sdu.dk

while the all-orders beta function [19,20] predicts the anomalous dimension of the mass to be unity for $N_f = 2.86$ we expect that chiral symmetry breaks for two Dirac flavors. However, we want to confirm here this result via first principle lattice simulations. Furthermore, there is also the possibility that the theory shows a certain degree of walking [9,10,21–23] unless the phase transition is of jumping type [24,25]. Jumping conformal phase transitions have been demonstrated to occur in a wide class of theories [26].

As a natural first step, we study the phase diagram in the (β, m_0)-plane to find the relevant region of parameter space to simulate. We then determine the zero partial conservation of the axial current (PCAC) mass line as well as the strong coupling bulk phase transition line. In addition, we report on the pseudoscalar, vector and axial vector meson masses. From the measured spectrum we infer that the theory breaks chiral symmetry dynamically. Part of these results appeared in Ref. [27].

In Sec. II we present the analytic expectations for the phase diagram of SO(N) as a function of the number of flavors. We also summarize the expected breaking pattern of the quantum global symmetries for theories below the conformal window. We also prove the spectral degeneracy between certain diquarks and ordinary mesonlike states. In Sec. III we recall the lattice formulation of the theory and summarize the physical observable studied here. The results of the simulations are reported in Sec. IV and conclude in Sec. V.

II. ORTHOGONAL CONFORMAL WINDOW AND CHIRAL SYMMETRY BREAKING PATTERN

The two loop β-function for an SO(N) theory with N_{f} Dirac fermions transforming according to the vector representation of the gauge group is

$$\beta(\alpha) = -\frac{\alpha^2}{2\pi}\left(b_0 + b_1\frac{\alpha}{2\pi}\right), \tag{1}$$

where

$$\begin{aligned} b_0 &= \frac{11}{3}N_{\mathrm{c}} - \frac{4}{3}N_{\mathrm{f}} - \frac{22}{3}, \\ b_1 &= -\frac{10}{3}(N_{\mathrm{c}}-2)N_{\mathrm{f}} - (N_{\mathrm{c}}-1)N_{\mathrm{f}} + \frac{17}{3}(N_{\mathrm{c}}-2)^2. \end{aligned} \tag{2}$$

A naive estimate of the lower bound of conformal window is given when the second coefficient b_1 changes sign. For SO(4) this happens when $N_f = \frac{68}{29} \simeq 2.3$. The corresponding values for three and four-loops in the $\overline{\mathrm{MS}}$-scheme are $N_f = 1.8$ and $N_f = 3.0$. The all-orders beta function predicts as lower boundary $N_f = 2.86$, see Fig. 1. Hence, perturbative and nonperturbative methods suggest that chiral symmetry breaks for two Dirac flavors. However, lattice simulations can seal this expectation. Since the vector representations of orthogonal groups are real the quantum

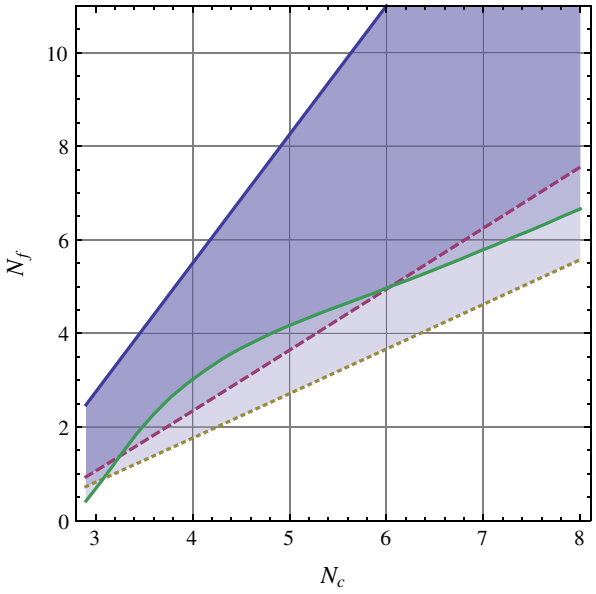

FIG. 1 (color online). Conformal window of SO(N_{c}) with N_{f} Dirac fermions in the fundamental representation. Upper bound is when asymptotic freedom is lost. Lower bounds are 2-loop (red, dashed), 3-loop (yellow, dotted) and 4-loop estimates (green, solid).

global symmetry of the theory is, for a generic N_f SU($2N_{\mathrm{f}}$) which is larger than SU(N)$_{\mathrm{f}}$ $\otimes$ SU(N_{f}) $\otimes$ U$_V$(1) valid for complex fermion representations. The reality property of the representation translates in the following property of the Dirac operator

$$(\not{D} + m)C\gamma^5 = C\gamma^5(\not{D} + m)^*, \tag{3}$$

where $\not{D} = \gamma^\mu(\partial_\mu - igA^a_\mu\tau_a)$, $a = 1, \ldots, d[G]$ where $d[G]$ is the dimension of the adjoint representation of the gauge group and $C = i\gamma^0\gamma^2$ is the charge conjugation operator.

The global SU($2N_{\mathrm{f}}$) is assumed to break to the maximal diagonal subgroup

$$\mathrm{SU}(2N_{\mathrm{f}}) \rightarrow \mathrm{SO}(2N_{\mathrm{f}}), \tag{4}$$

for the massless theory and for N_f below the conformal window. A common mass for the Dirac fermions leads to the same pattern of explicit symmetry breaking. The explicit interpolating operators for the Goldstones can be naturally divided in three independent antifermion-fermion bilinears

$$\bar{\psi}_f\gamma^5\psi_{f'}, \tag{5}$$

with f and f' the flavor indices $f = 1, 2$ and six *difermion* operators

$$\psi_f^T C\gamma^5\psi_{f'} \quad \text{and} \quad \bar{\psi}_f\gamma^5 C\bar{\psi}_{f'}^T. \tag{6}$$

The reader can find a useful summary of the global symmetry breaking patterns tailored for lattice computations in

Ref. [28], while applications to beyond standard model physics for similar patterns appeared in Refs. [17,29]. Notice that whereas the usual pions have odd parity, the corresponding diquarks are parity even. It was noticed in Ref. [9] that when fermions are in a pseudoreal representation, the diquark correlator is exactly identical to the corresponding mesonic correlator. In the Appendix we give a similar proof for fermions in real representations. The proof uses the symmetry (3) of the Dirac operator along with the γ^5-hermiticity $\gamma^5(\not{D}+m)\gamma^5=(\not{D}+m)^\dagger$ property. The result can be stated as

$$c^{(\Gamma)}_{\bar\psi_f\bar\psi_{f'}}(x-y)=c^{(\Gamma)}_{\bar\psi_f\psi_{f'}}(x-y)=c^{(\Gamma)}_{\psi_f\psi_{f'}}(x-y), \tag{7}$$

where $c^{(\Gamma)}_{\bar\psi_f\psi_{f'}}$ is the correlator for the operator $\bar\psi_f\Gamma\psi_{f'}$ and $c^{(\Gamma)}_{\psi_f\psi_{f'}}$ is the correlator for the corresponding diquark operator $\psi_f^T\Gamma C\psi_{f'}$. Γ can be any of the matrices $\mathbf{1}$, γ^5, γ^μ, $\gamma^\mu\gamma^5$.

Having discussed the generic features expected for orthogonal groups we now turn to the lattice formulation and results for the relevant case of SO(4) with two Dirac flavors.

III. LATTICE FORMULATION

In this work we have used the Wilson prescription for the lattice action

$$S=S_{\rm F}+S_{\rm G}, \tag{8}$$

where

$$S_{\rm G}=\beta\sum_x\sum_{\mu,\nu<\mu}\left[1-\frac{1}{N_{\rm c}}\,{\rm Tr}\,\mathcal{U}_{\mu\nu}(x)\right], \tag{9}$$

is the Yang-Mills gauge action. We have normalized the lattice spacing to $a=1$. $\mathcal{U}_{\mu\nu}(x)$ is the plaquette defined in terms of the link variables as

$$\mathcal{U}_{\mu\nu}(x)=\mathcal{U}_\mu(x)\mathcal{U}_\nu(x+\hat\mu)\mathcal{U}^T_\mu(x+\hat\mu+\hat\nu)\mathcal{U}^T_\nu(x+\hat\nu). \tag{10}$$

The Wilson fermion action is

$$S_{\rm F}=\sum_f\sum_{x,y}\bar\psi_f(x)M(x,y)\psi_f(y), \tag{11}$$

with f running over fermion flavors and the Wilson-Dirac matrix $M(x,y)$ given by

$$\begin{aligned}\sum_y M(x,y)\psi(y)&=(4+m_0)\psi(x)\\&-\frac{1}{2}\sum_\mu\Big[(1+\gamma_\mu)\mathcal{U}^T_\mu(x-\hat\mu)\psi(x-\hat\mu)\\&+(1-\gamma_\mu)\mathcal{U}_\mu(x)\psi(x+\hat\mu)\Big].\end{aligned} \tag{12}$$

Here the gauge and spinor indices have been suppressed. The bare parameters are the inverse of the bare coupling $\beta=2N_{\rm c}/g_0^2$ appearing in the gauge action and the bare mass m_0 of the Wilson fermions.

We employ the PCAC relation to define the physical quark mass

$$m_{\rm PCAC}=\lim_{t\to\infty}\frac{1}{2}\frac{\partial_t V_{\rm PS}}{V_{\rm PP}}, \tag{13}$$

where the currents are

$$\begin{aligned}V_{\rm PS}(x_0)&=a^3\sum_{x_1,x_2,x_3}\langle\bar\psi_1(x)\gamma_0\gamma_5\psi_2(x)\bar\psi_1(0)\gamma_5\psi_2(0)\rangle,\\V_{\rm PP}(x_0)&=a^3\sum_{x_1,x_2,x_3}\langle\bar\psi_1(x)\gamma_5\psi_2(x)\bar\psi_1(0)\gamma_5\psi_2(0)\rangle.\end{aligned} \tag{14}$$

The meson masses are estimated using time slice averaged zero momentum correlators

$$C^{(\Gamma)}_{\bar\psi_1\psi_2}(x_0)=a^3\sum_{x_1,x_2,x_3}{\rm Tr}([\bar\psi_1(x)\Gamma\psi_2(x)]^\dagger\,\bar\psi_1(0)\Gamma\psi_2(0)), \tag{15}$$

where $\Gamma=\gamma_5$ for pseudoscalar, $\Gamma=\gamma_k$ ($k=1,2,3$) for vector, and $\gamma_5\gamma_k$ for axial vector meson.

IV. RESULTS

The simulations were performed on three different lattices $8^3\times16$, $12^3\times64$ and $24^3\times64$ where in all cases the larger dimension is the temporal one. All the simulations were started from a random configuration and the first 500–2000 iterations were discarded. This is enough to thermalize the system for the quantities we measured. For a complete list of the simulations see Table I where we have omitted the values of the bare masses.

The smallest lattice was used for exploration of the parameter space spanned by the bare mass m_0 and the coupling β. Figure 2 shows an outline of the lattice phase structure measured on this $8^3\times16$ lattice. For small values of β the system is in a bulk phase not connected to continuum physics. The bulk phase is separated from the small coupling (large β) phase by a first order phase transition. Figure 3 shows the discontinuous behavior of

TABLE I. Simulation parameters and thermalization times. For each coupling we performed multiple simulations with appropriate bare masses. The thermalization column refers to the number of discarded initial configurations.

Volume	β	Iterations	Thermalization
$8^3\times16$	4.1, 4.2, ..., 4.9, 5.2, 5.4, 5.6	2000	500
	44.55, 5.5, 6, 7	5000	2000
$12^3\times64$	5.5, 7	5000	1500
$24^3\times64$	7	850–2000	600

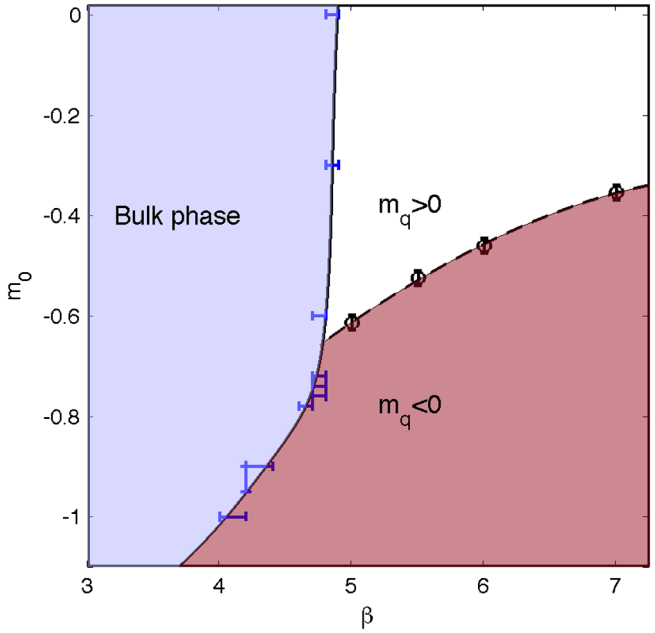

FIG. 2 (color online). Lattice phase structure outlined on an $8^3 \times 16$ lattice. Circles represent points of critical bare mass where $m_{\mathrm{PCAC}} = 0$. The transition between the bulk phase is of first order. The error bars represent the interval over which the measured average plaquette jumps.

the average plaquette when crossing the bulk phase transition, for three different values of m_0. The uncertainty on the location of the bulk phase transition shown in Fig. 2 is due to taking discrete values of β between simulation points.

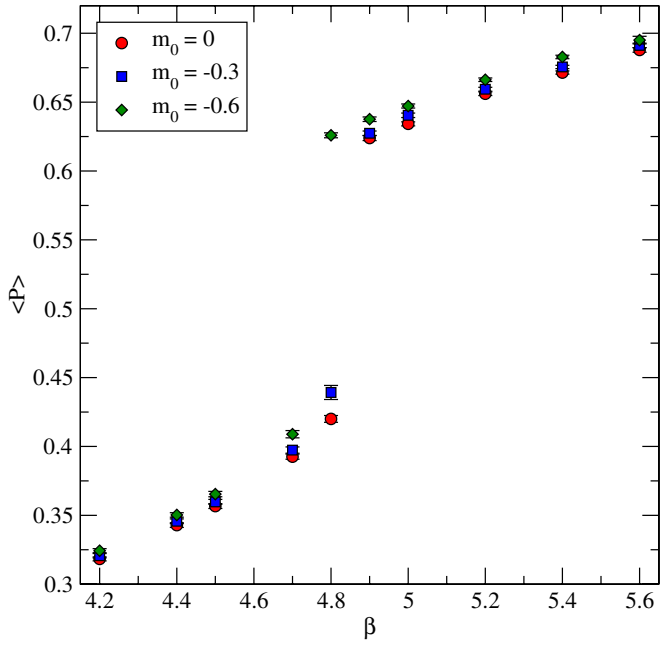

FIG. 3 (color online). Average plaquette $\langle P \rangle$ vs β on an $8^3 \times 16$ lattice at three different values of the bare mass.

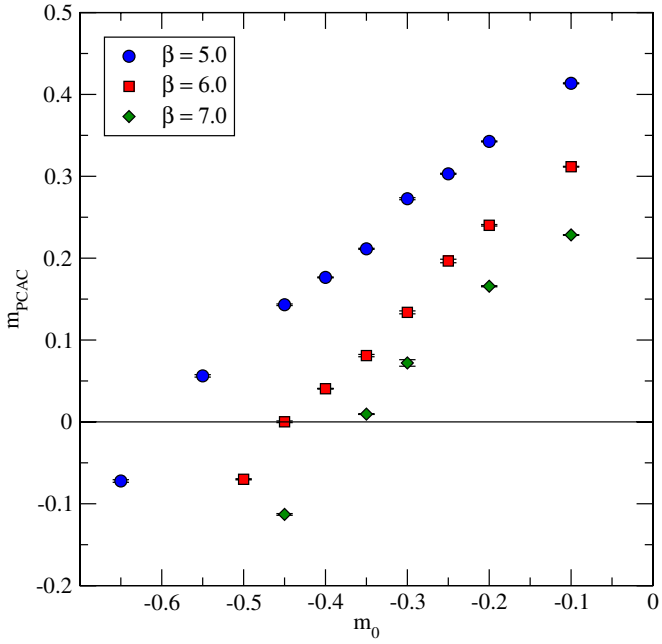

FIG. 4 (color online). m_{PCAC} in units of inverse lattice spacing at three different couplings. The measurements are performed on a $8^3 \times 16$.

We can compare our result for the location of the bulk transition to previous studies of SO(N) pure gauge theories. Earlier simulations focused mainly on the SO(3) gauge group [30] with the exception of Ref. [31] where also other values of N were considered. For SO(4) the authors of Ref. [31] find that the bulk phase transition happens for $4.62(3) < \beta < 4.87(3)$, which is in agreement with our result in Fig. 3.

The critical line where the physical quark mass vanishes is determined from the PCAC relation (13). The critical line of $m_q = 0$ in the phase diagram (Fig. 2) is constructed by linear fits to the PCAC mass. Figure 4 shows the bare mass dependency of the PCAC mass at three different couplings on the $8^3 \times 16$ lattice.

A. Finite size effects

According to the perturbative estimates discussed in Sec. II the running of the gauge coupling is expected to be slow. This also suggests that attention should be paid to finite size effects, which need to be estimated nonperturbatively by measuring physical observables as a function of lattice size.

In the case of SO(N) pure gauge theories [30,31] the bulk phase transition occurs at such a weak coupling that extremely large lattices are required for simulations in the confined phase, the one connected to the continuum physics. However, in the presence of dynamical quarks, we find that somewhat smaller volumes ($24^3 \times 64$) are enough to probe the chiral regime of the system.

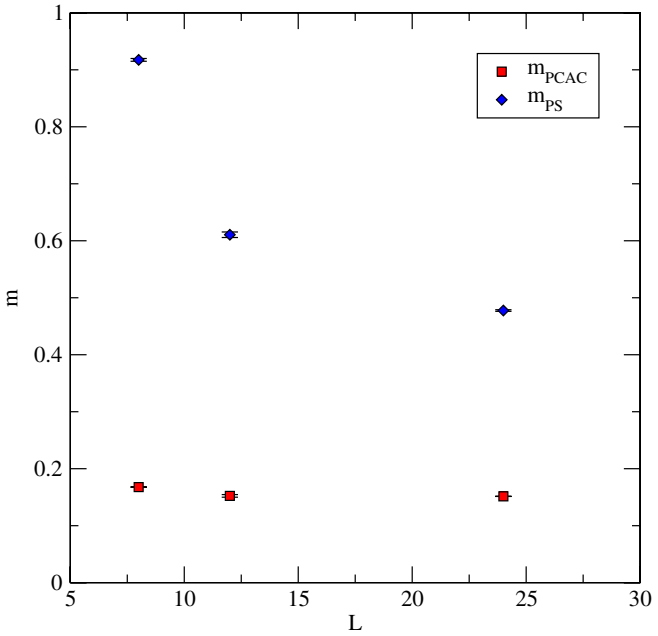

FIG. 5 (color online). Finite size effects on m_{PS} and m_{PCAC} in units of inverse lattice spacing. The measurements are performed on a $24^3 \times 64$ lattice at $\beta = 7$ and $m_0 = -0.2$.

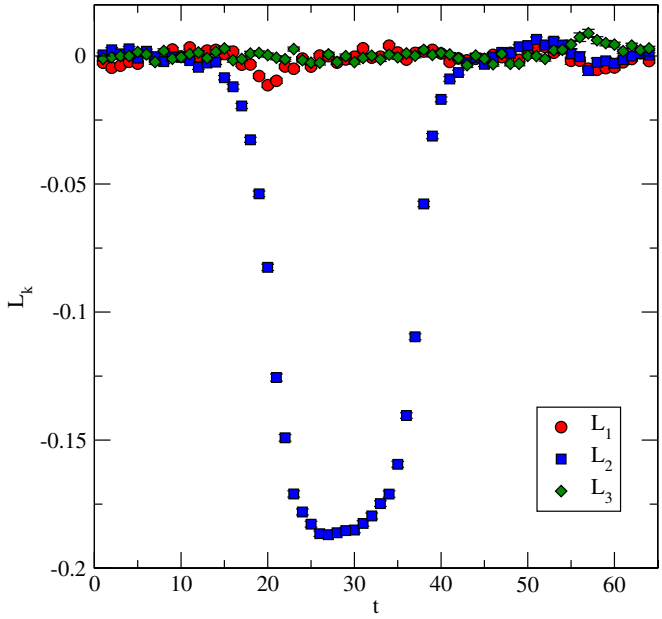

FIG. 6 (color online). Average Polyakov loops wound around the three spatial dimensions computed at each time slice of the lattice. This measurement was performed on a $12^3 \times 64$ lattice at $\beta = 7$ and $m_0 = -0.3$. The values are averages over 700 configurations starting at 1800 where the system does not appear to thermalize further.

In Fig. 5 the mass of the pseudoscalar meson m_{PS} and the PCAC quark mass m_{PCAC} is plotted for different lattice sizes. The PCAC mass has little dependence on the lattice size being a UV quantity. The pseudoscalar meson mass, on the contrary, is very sensitive to finite size effects even if it is still somewhat heavy at the bare mass used in Fig. 5.

Another interesting property which seems to occur at small volumes is a phase separation characterized by the existence of domain walls. As explained below, this would be different from what happens in simulations of SU(N) gauge models in the so-called femto-world regime [32–34].

We observe the coexistence, inside the same 4-volume, of two distinct phases which can be characterized by the spatial average of Polyakov loops wrapping around the three spatial directions taken on each time slice separately. In detail, the operators we consider are defined as

$$L_k(t) = \left\langle \frac{1}{N_i N_j} \sum_{x_i, x_j} \frac{1}{N} \mathrm{Tr} \prod_{x_k} \mathcal{U}_k(t, \mathbf{x}) \right\rangle, \qquad (16)$$

where $i \neq j \neq k$ are spatial directions. The two phases are separated by domain walls which are stable for the whole length of our simulations, of the order of ~5000 hybrid Monte Carlo updates. As an illustration of this phenomenon, Fig. 6 shows the time resolved Polyakov loops on a $12^3 \times 64$ lattice at $\beta = 7$ and $m_0 = -0.3$. Given that the two phases are long-lived and do not move inside the 4-volume of the lattice during the simulation, we show the average of the time-resolved Polyakov loops over 700 consecutive, thermalized configurations. The coexistence of two phases with different values of L_2 is clear from the figure. The phenomenon appears in all simulations performed on small lattices. The location of the phase boundaries and the direction in which the Polyakov loop has nonzero average is random. In some cases more than two phase boundaries appear in the same system. Notice also that in one of the two phases the average value of the Polyakov loop vanishes.

The behavior just described for this model is in contrast with what is normally observed in simulations done with SU(N) gauge groups in a small boxes. In the so-called femto-world regime of SU(N) gauge theories, one also expects the Polyakov loops to spontaneously generate a nonvanishing expectation value, but stable domain walls inside the lattice volume are not observed.

The coexistence of two phases is also reflected in an anomalous behavior of mesonic correlators measured for volumes smaller than $24^3 \times 64$. An example is shown in Fig. 7 where the effective mass plateaux of the pseudoscalar meson shows a visible rise at large separations, consistent with the two phases having different pseudoscalar correlation lengths.

In order to understand whether these phase separations are related to the presence of dynamical fermions we have also performed pure gauge simulations on $12^3 \times 64$ lattices. The phase separation occurs also for the pure gauge. Thus the phenomenon seems to be a feature stemming from the pure gauge sector.

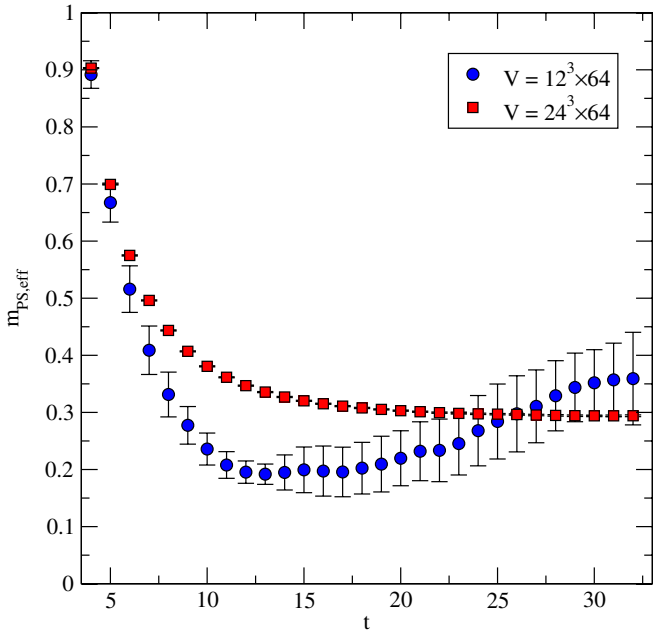

FIG. 7 (color online). Effective mass of pseudoscalar meson for two different volumes.

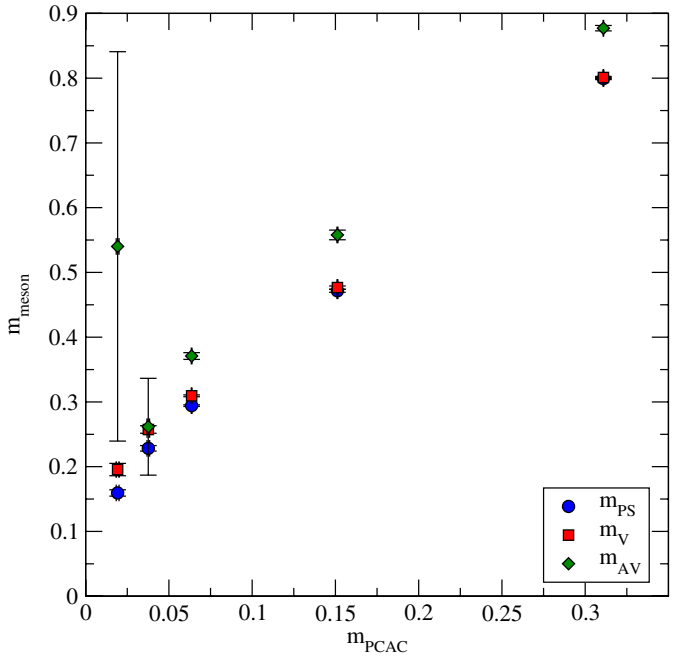

FIG. 8 (color online). Pseudoscalar, vector, and axial vector meson masses measured on a $24^3 \times 64$ lattice at $\beta = 7$.

We will not explore this feature further in this work, but it would be interesting to continue its investigation in the future.

In order to avoid the complications stemming from the phase separation described above we use $24^3 \times 64$ lattices for the rest of the paper.

B. Spectrum and chiral symmetry breaking

We address the dynamical fate of the chiral symmetries of the theory by determining the pseudoscalars and (axial) vectors spectrum.

Figure 8 shows the pseudoscalar, vector, and axial vector meson masses measured on a $24^3 \times 64$ lattice at $\beta = 7$ as the bare quark mass is decreased towards the critical value. At the lightest quark mass the pseudoscalar meson has a mass of about $m_{\mathrm{PS}} \simeq 0.15$ in lattice units corresponding to about $m_{\mathrm{PS}}L \simeq 3.6$. Since two of the three volumes used in this study are affected by the presence of the phase separation phenomenon discussed above, it is difficult to estimate the finite volume effect on the light states. However, we will take the values of the pseudoscalar and vector masses obtained here as reasonable first estimates and leave a more systematic investigation of the finite volume effects for the future. The reader should also be aware that in previous studies of non-QCD models such as the so-called sextet model [35] or MWT [36] it was found that larger values of $m_{\mathrm{PS}}L$ than in QCD are needed to accurately measure the light states.

At large quark masses the vector and pseudoscalar are degenerate with the common mass increasing linearly with the quark mass. At smaller masses the vector meson becomes heavier than the pseudosclar. This is consistent with dynamical generation of a chiral scale. To see this more clearly the ratio of the vector and the pseudoscalar masses have been plotted in Fig. 9. Indeed the mass ratio approaches unity for large quark masses. However, when approaching the chiral limit the ratio increases signaling chiral symmetry breaking. In fact this result is consistent with the expectation that if spontaneous

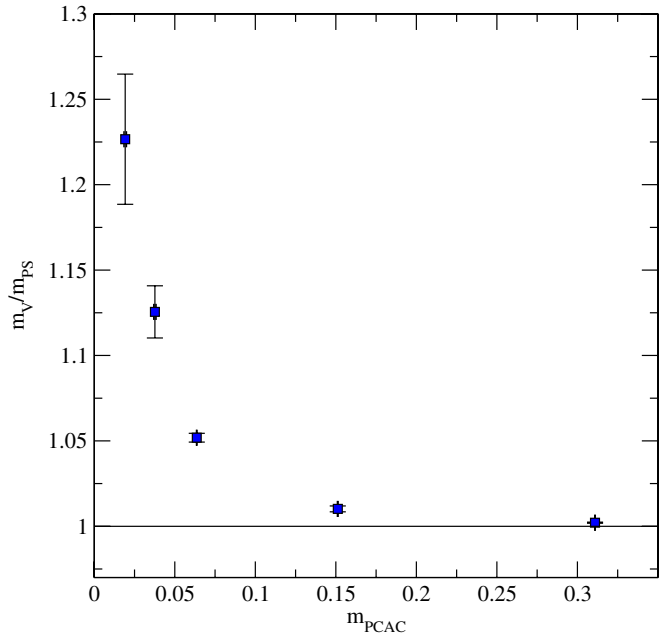

FIG. 9 (color online). Ratio between pseudoscalar and vector meson masses measured on a $24^3 \times 64$ lattice at $\beta = 7$.

symmetry breaking occurs, the vector meson remains massive whereas the pseudoscalar meson is massless. A diverging ratio m_V/m_{PS} therefore indicates chiral symmetry breaking. This is the trend we observe in Fig. 9. However to nail this conclusion more studies have to be performed.

The axial mass in the chiral limit is poorly determined Fig. 8. In the future we plan on improving its determination. We will then be able to use it to infer interesting properties of the chiral transition. For example one can investigate whether the axial remains (near) degenerate with the vector in the chiral regime which could signify the onset of walking dynamics [29,37].

To extract further properties of the theory we analyze in more detail the functional dependence of the pseudocalar mass on the quark mass. It is well known that, for these kinds of theories, spontaneously broken chiral symmetry leads to the Gell-Mann-Oakes-Renner relation [38]

$$m_{PS}^2 \simeq \Lambda m_{PCAC}, \tag{17}$$

valid in the chiral limit, where $\Lambda = -2\langle\bar{\psi}\psi\rangle/f_{PS}^2$ is a dynamically generated scale. For conformal theories the behavior is different [39,40]. In Ref. [40] it was also shown that the instanton contributions to conformal chiral dynamics can be neglected when the anomalous dimension of the mass operator is less than one. This property has been investigated and confirmed via lattice simulations in Ref. [41]. A clever separation of the ultraviolet and infrared modes presented in Refs. [42,43] led to a better understanding of the conformal chiral scenario but without discussing the instanton contributions [40]. Building upon these results, an interesting method to determine the anomalous dimension of the fermion masses was put forward in Ref. [44]. To sum up, for a conformal scenario the dynamical scale Λ mutates into a fermion-mass dependent quantity [40] and therefore m_{PS}^2 must vanish as m_{PCAC}^2. In Fig. 10 we plot the ratio m_{PS}^2/m_{PCAC} for decreasing fermion mass. We see that the ratio approaches a constant for vanishing fermion masses which is consistent with the chiral symmetry breaking scenario (17).

TABLE II. Different types of fit functions in the chiral regime for the data with m identified with the m_{PCAC}.

Meson fit	Fit function	Best parameter	χ^2/dof
ps chiral	$a\sqrt{m}$	$a = 1.167(6)$	0.43/2
ps conformal	am	$a = 4.69(3)$	364/2
ps alternative 1	$a + bm$	$a = 0.111(6)$	6.4/1
		$b = 2.9(1)$	
ps alternative 2	$a + b\sqrt{m}$	$a = -0.001(10)$	0.41/1
		$b = 1.17(4)$	
Vector chiral	$a + bm$	$a = 0.16(1)$	3.3/1
		$b = 2.3(2)$	
Vector conformal	am	$a = 4.91(3)$	273/2
Vector alternative 1	$a\sqrt{m}$	$a = 1.231(6)$	18/2
Vector alternative 2	$a + b\sqrt{m}$	$a = 0.07(2)$	0.69/1
		$b = 0.96(7)$	

In Table II we report the fit to the data for the dependence of the pseudoscalar mass as well as the vector mass as a function of the m_{PCAC} within the believed chiral regime of the theory. This corresponds to the three lowest values of m_{PCAC} where the ratio m_{PS}^2/m_{PCAC} becomes roughly constant as shown in Fig. 10. The data points used for the chiral fits in the table are shown in Fig. 11.

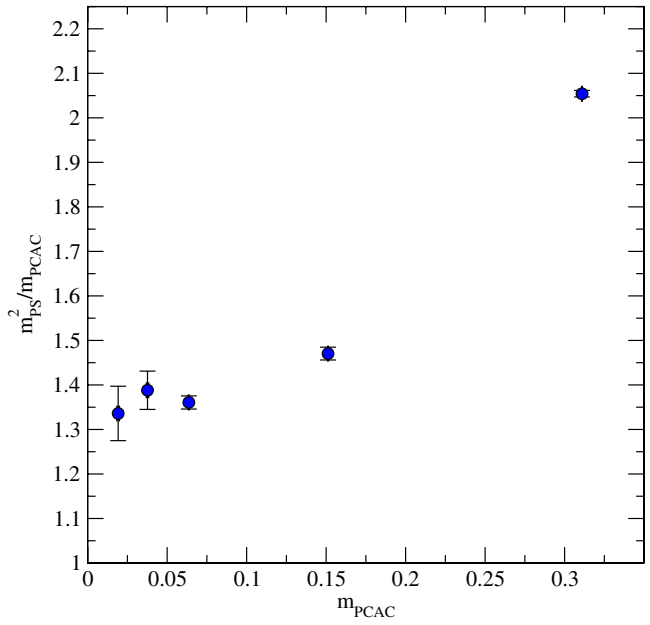

FIG. 10 (color online). Psudoscalar mass squared divided by the quark mass measured on a $24^3 \times 64$ lattice at $\beta = 7$.

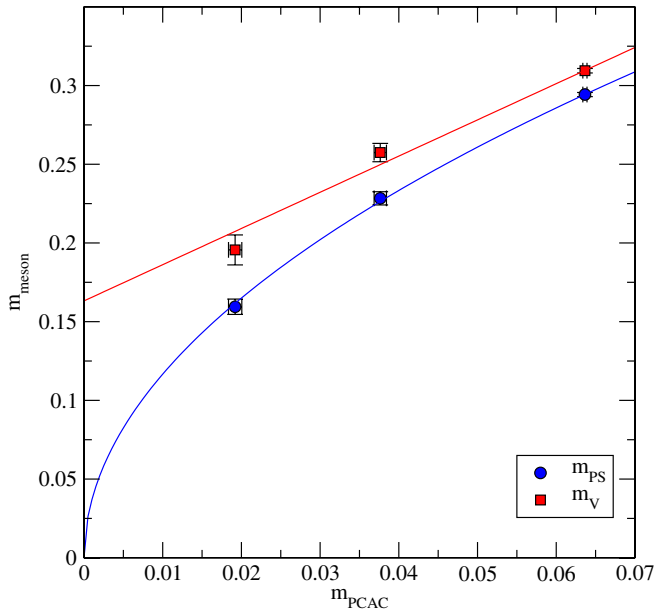

FIG. 11 (color online). The chiral fits to the pseudo scalar and vector meson masses on a $24^3 \times 64$ lattice at $\beta = 7$.

For these three points we have $f_{\mathrm{PS}}L \approx 0.8$–$0.9$. The best fit curve, determined by the lowest χ^2/dof, for the pseudoscalar mass corresponds to the first line of the table which is in agreement with the GMOR expectation. It is remarkable that by even allowing for an offset of the mass value in the chiral limit the best fit demands the offset to vanish, see the last line of the table. We have tried also to test the possibility that the pseudoscalar mass vanishes linearly with the fermion mass and found that this is highly disfavored. If the theory would have been conformal we would have expected this case to fit much better.

Similarly, by fitting the vector masses dependence on the fermion mass, in the lower part of Table II, we observe a reasonable agreement with the expected chiral behavior of the theory. The two best fits correspond to the first and last line of the lower part of the table. We would have expected the first line to yield a better fit if chiral symmetry breaks like in ordinary quantum chromodynamics. We believe that for this case more statistics is needed to resolve which of the two cases is actually realized given that the data cannot yet differentiate between the two. As for the pseudoscalar case the would-be conformal case is highly disfavored (see second line of the lower part of the table).

Using the identity for the hadronic correlators (8) we can immediately infer the baryonic diquark masses.

V. CONCLUSIONS

Orthogonal lattice gauge theories with dynamical fermions have so far been *terra incognita*. However, as explained in the introduction, these theories can be relevant for models of dynamical electroweak symmetry breaking as well as for the construction of interesting dark matter candidates. Furthermore to have a deeper understanding of strong dynamics it is essential to gain information on different gauge theories. We have chosen to start investigating the orthogonal gauge groups dynamics with a phenomenologically relevant example, i.e., the SO(4) gauge theory with two Dirac flavors transforming according to the vector representation of the group.

We have uncovered the lattice phase diagram and shown that there is a novel phase separation phenomenon at small volumes which persists even in the pure gauge case. We have shown that the phase separation can be circumvented and the chiral regime of the theory studied using large but still feasible lattices.

Finally we investigated the spectrum of the theory for the pseudoscalar, vectors and axial vectors. The results for the spectrum are consistent with chiral symmetry breaking and strongly disfavor a conformal behavior. The spectrum was obtained using lattices with a fixed value of the UV cutoff, corresponding to $\beta = 7$. Further investigations will be needed using different values of the cutoff to better address the continuum limit.

APPENDIX: DIQUARK CORRELATORS

A generic mesonic correlator will have the form

$$c^{(\Gamma)}_{\bar{\psi}\psi'}(x-y) = \mathrm{Tr}([\bar{\psi}(x)\Gamma\psi'(x)]^\dagger\,\bar{\psi}(y)\Gamma\psi'(y)), \tag{A1}$$

and the baryonic diquark correlator will have the form

$$c^{(\Gamma)}_{\psi\psi'}(x-y) = \mathrm{Tr}([\psi^T(x)C\Gamma\psi'(x)]^\dagger\,\psi^T(y)C\Gamma\psi'(y)). \tag{A2}$$

Rewriting the diquark correlator slightly gives

$$c^{(\Gamma)}_{\psi\psi'}(x-y) = \mathrm{Tr}(\Gamma\psi'(y)\bar{\psi}'(x)\gamma^0\Gamma^\dagger C^\dagger(\gamma^0)^T \times[\psi(y)\bar{\psi}(x)]^T C). \tag{A3}$$

Now we can invoke two identities

$$(\gamma^\mu)^T = -C\gamma^\mu C^\dagger, \tag{A4}$$

$$\psi(x)\bar{\psi}(y) = C^\dagger[\psi(y)\bar{\psi}(x)]^T C. \tag{A5}$$

The latter identity follows from the symmetry of the Dirac matrix given in (3) along with γ^5-hermiticity $\gamma^5(\not{D}+m)\gamma^5 = (\not{D}+m)^\dagger$. The identity (A5) extend to the Wilson lattice formulation of the Dirac matrix. This is demonstrated for pseudoreal representations in the Appendix of Ref. [9]. Invoking the identities in the expression for the diquark correlator (A3) we have

$$\begin{aligned} c^{(\Gamma)}_{\psi\psi'}(x-y) &= \mathrm{Tr}(\Gamma\psi'(y)\bar{\psi}'(x)\gamma^0\Gamma^\dagger\gamma^0\psi(x)\bar{\psi}(y)) \\ &= c^{(\Gamma)}_{\bar{\psi}\psi'}(x-y). \end{aligned} \tag{A6}$$

A similar derivation holds for the antiparticles leading to the identity (8).

[1] F. Sannino, arXiv:0804.0182.
[2] P. Channuie, J. J. Joergensen, and F. Sannino, J. Cosmol. Astropart. Phys. 05 (2011) 007.
[3] F. Bezrukov, P. Channuie, J. J. Joergensen, and F. Sannino, Phys. Rev. D **86**, 063513 (2012).
[4] P. Channuie, J. J. Joergensen, and F. Sannino, Phys. Rev. D **86**, 125035 (2012).
[5] F. Sannino and K. Tuominen, Phys. Rev. D **71**, 051901 (2005).
[6] D. D. Dietrich and F. Sannino, Phys. Rev. D **75**, 085018 (2007).
[7] F. Sannino, Phys. Rev. D **79**, 096007 (2009).
[8] M. Mojaza, C. Pica, T. A. Ryttov, and F. Sannino, Phys. Rev. D **86**, 076012 (2012).

[9] R. Lewis, C. Pica, and F. Sannino, Phys. Rev. D **85**, 014504 (2012).
[10] M. T. Frandsen and F. Sannino, Phys. Rev. D **81**, 097704 (2010).
[11] S. Weinberg, Phys. Rev. D **19**, 1277 (1979).
[12] L. Susskind, Phys. Rev. D **20**, 2619 (1979).
[13] D. D. Dietrich, F. Sannino, and K. Tuominen, Phys. Rev. D **72**, 055001 (2005).
[14] R. Foadi, M. T. Frandsen, T. A. Ryttov, and F. Sannino, Phys. Rev. D **76**, 055005 (2007).
[15] E. Witten, Phys. Lett. **117B**, 324 (1982).
[16] E. Del Nobile, C. Kouvaris, and F. Sannino, Phys. Rev. D **84**, 027301 (2011).
[17] S. B. Gudnason, C. Kouvaris, and F. Sannino, Phys. Rev. D **73**, 115003 (2006).
[18] T. A. Ryttov and F. Sannino, Phys. Rev. D **78**, 115010 (2008).
[19] T. A. Ryttov and F. Sannino, Phys. Rev. D **78**, 065001 (2008).
[20] C. Pica and F. Sannino, Phys. Rev. D **83**, 116001 (2011).
[21] B. Holdom, Phys. Rev. D **24**, 1441 (1981).
[22] K. Yamawaki, M. Bando, and K. i. Matumoto, Phys. Rev. Lett. **56**, 1335 (1986).
[23] T. W. Appelquist, D. Karabali, and L. C. R. Wijewardhana, Phys. Rev. Lett. **57**, 957 (1986).
[24] F. Sannino, arXiv:1205.4246.
[25] P. de Forcrand, S. Kim, and W. Unger, arXiv:1208.2148.
[26] O. Antipin, M. Mojaza, and F. Sannino, arXiv:1208.0987.
[27] A. Hietanen, C. Pica, F. Sannino, and U. I. Sondergaard, Proc. Sci. LATTICE2012 (2012) 065.
[28] J. B. Kogut, M. A. Stephanov, D. Toublan, J. J. M. Verbaarschot, and A. Zhitnitsky, Nucl. Phys. **B582**, 477 (2000).
[29] T. Appelquist, P. S. Rodrigues da Silva, and F. Sannino, Phys. Rev. D **60**, 116007 (1999).
[30] P. de Forcrand and O. Jahn, Nucl. Phys. **B651**, 125 (2003).
[31] F. Bursa, R. Lau, and M. Teper, arXiv:1208.4547.
[32] M. Luscher, Nucl. Phys. **B219**, 233 (1983).
[33] P. van Baal, Commun. Math. Phys. **94**, 397 (1984).
[34] J. Koller and P. van Baal, Nucl. Phys. **B302**, 1 (1988).
[35] Z. Fodor, K. Holland, J. Kuti, D. Nogradi, and C. Schroeder, arXiv:1103.5998.
[36] A. Patella, L. Del Debbio, B. Lucini, C. Pica, and A. Rago, Proc. Sci. LATTICE2011 (2011) 084.
[37] T. Appelquist and F. Sannino, Phys. Rev. D **59**, 067702 (1999).
[38] M. Gell-Mann, R. J. Oakes, and B. Renner, Phys. Rev. **175**, 2195 (1968).
[39] F. Sannino and R. Zwicky, Phys. Rev. D **79**, 015016 (2009).
[40] F. Sannino, Phys. Rev. D **80**, 017901 (2009).L. Del Debbio, B. Lucini, A. Patella, C. Pica, and A. Rago, Phys. Rev. D **80**, 074507 (2009).
[41] E. Bennett and B. Lucini, arXiv:1209.5579.
[42] L. Del Debbio and R. Zwicky, Phys. Rev. D **82**, 014502 (2010).
[43] L. Del Debbio and R. Zwicky, Phys. Lett. B **700**, 217 (2011).
[44] A. Patella, Phys. Rev. D **84**, 125033 (2011).